



HAL
open science

Hydrodynamic and suspended sediment transport controls on river mouth morphology

F. Falcini, A. Piliouras, R. Garra, A. Guerin, D. J. Jerolmack, J. Rowland, C.
Paola

► **To cite this version:**

F. Falcini, A. Piliouras, R. Garra, A. Guerin, D. J. Jerolmack, et al.. Hydrodynamic and suspended sediment transport controls on river mouth morphology. *Journal of Geophysical Research: Earth Surface*, 2014, 119, pp.1-11. 10.1002/2013JF002831 . insu-03581155

HAL Id: insu-03581155

<https://insu.hal.science/insu-03581155>

Submitted on 19 Feb 2022

HAL is a multi-disciplinary open access archive for the deposit and dissemination of scientific research documents, whether they are published or not. The documents may come from teaching and research institutions in France or abroad, or from public or private research centers.

L'archive ouverte pluridisciplinaire **HAL**, est destinée au dépôt et à la diffusion de documents scientifiques de niveau recherche, publiés ou non, émanant des établissements d'enseignement et de recherche français ou étrangers, des laboratoires publics ou privés.

Copyright

Hydrodynamic and suspended sediment transport controls on river mouth morphology

F. Falcini,¹ A. Piliouras,² R. Garra,³ A. Guerin,⁴ D. J. Jerolmack,⁵ J. Rowland,⁶ and C. Paola⁷

Received 18 April 2013; revised 6 November 2013; accepted 7 November 2013; published 14 January 2014.

[1] River mouths building into standing bodies of water have strikingly varied growth habits. This presents a compelling pattern formation problem that is also of great practical relevance for subsurface prediction and managing coastal wetlands. Here we present a generalized 2.5-dimensional potential vorticity (PV) theory that explains sedimentation patterns of a sediment-laden stationary jet by coupling an understanding of vorticity with suspended sediment concentration fields. We explore the physical meaning of this new sediment-PV definition, and its impact on outflow depositional patterns, by analyzing data from a shallow wall-bounded plane jet experiment and by discussing new theoretical insights. A key result is that lateral advection and diffusion of suspended sediment are directly proportional to jet vorticity, a feature that reveals the mechanistic process that forms elongated channels by focused levee deposition. The new PV theory constitutes a more generalized mathematical framework that expands the Rouse theory for the equilibrium of suspended sediment.

Citation: Falcini, F., A. Piliouras, R. Garra, A. Guerin, D. J. Jerolmack, J. Rowland, and C. Paola (2014), Hydrodynamic and suspended sediment transport controls on river mouth morphology, *J. Geophys. Res. Earth Surf.*, 119, 1–11, doi:10.1002/2013JF002831.

1. Introduction

[2] The growth patterns of river deltas are important for a variety of reasons. Deltaic deposits host much of the world's hydrocarbon resources and provide templates for understanding delta growth under a wide range of natural conditions. With increasing rates of sea level rise, human-accelerated land subsidence, and large-scale alteration of water and sediment supply, many of the world's heavily populated river deltas are threatened with irreversible land loss [Syvitski and Saito, 2007; Blum and Roberts, 2009; Syvitski et al., 2009]. This problem is acute on the Mississippi Delta, where scientists are proposing artificial diversions that would harness natural

land-building processes in order to mitigate wetland loss in the vicinity of New Orleans [Day et al., 2000; Kim et al., 2009a; Falcini et al., 2012]. Although river sediment discharge generally dictates the bulk efficiency of land building on a delta [Nittrouer, 1999; Blum and Tornqvist, 2000; Paola, 2000; Kim et al., 2009b; Paola et al., 2011], river mouth sedimentation patterns vary widely as a function of outflow hydrodynamics and sediment characteristics [e.g., Bates, 1953; Abramovich, 1963; Rajaratnam, 1976; Wright, 1977; Wang, 1984; Syvitski et al., 1998; Peckham, 2008, and references therein].

[3] Prograding deltas are formed by the deposition of sediment by the river at its mouth. Deposition can occur at the lateral margins of the channel outlet, as subaqueous levees, and/or at the center of the channel, as a mouth bar. Stronger levee deposition encourages formation of elongate channels, while stronger aggradation of a mouth bar yields bifurcating channels and thus branching networks [Wright, 1977; Edmonds and Slingerland, 2007]. Mouth bar aggradation processes are associated with quasi-radially symmetric deltas advancing into standing water [Parker et al., 1998; Kostic and Parker, 2003]. This latter form has been viewed as a reference pattern for delta restoration [Edmonds and Slingerland, 2007; Kim et al., 2009a]. It is therefore clear that understanding the relations between river mouth morphology and outflow hydrodynamics is critical for designing effective delta restoration schemes, e.g., characteristics of a river diversion. Recently, progress has been made on two fronts: (1) detailed morphodynamic simulations have reproduced a diverse range of river mouth morphologies by systematically varying flow, channel mouth geometry and sediment characteristics, e.g., cohesiveness [Edmonds and Slingerland, 2007, 2010] and (2) laboratory tank experiments

¹Istituto di Scienze dell' Atmosfera e del Clima, Consiglio Nazionale delle Ricerche, Rome, Italy.

²Department of Geological Sciences, University of Texas, Austin, Texas, USA.

³Dipartimento di Scienze di Base e Applicate per l'Ingegneria, "Sapienza" University, Rome, Italy.

⁴Equipe de Dynamique des Fluides Géologiques, Institut de Physique du Globe de Paris, Université Paris Diderot, Paris, France.

⁵Department Earth and Environmental Science, University of Pennsylvania, Philadelphia, Pennsylvania, USA.

⁶Earth and Environmental Sciences Division, Los Alamos National Laboratory, Los Alamos, New Mexico, USA.

⁷Department of Geology and Geophysics, University of Minnesota, Minneapolis, Minnesota, USA.

Corresponding author: F. Falcini, Istituto di Scienze dell' Atmosfera e del Clima, Consiglio Nazionale delle Ricerche, Rome, Italy. (f.falcini@isac.cnr.it)

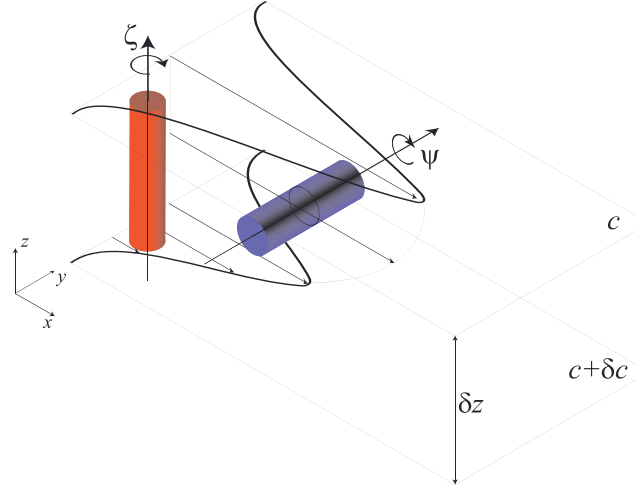


Figure 1. Schematic representation of the vorticity field $\vec{\omega} = (0, \psi, \zeta)$ in a sediment-laden, stratified jet, where the vorticity components $\psi = \partial u / \partial z$ and $\zeta = \partial v / \partial x - \partial u / \partial y$ are indicated by the blue and red cylinders, respectively. The bold lines are the horizontal velocity profile at two different depths; thin arrows indicate velocities on both horizontal and vertical planes. The horizontal planes along z represent suspended sediment stratification.

have empirically determined the conditions under which focused subaqueous levee deposition occurs at a river mouth, helping to understand the hydrodynamics leading to the formation of elongate channels [Rowland *et al.*, 2009, 2010].

[4] Inspired by this progress, Falcini and Jerolmack [2010, hereafter FJ10] proposed an analytical approach to describe the different delta morphologies. The basis of this approach was a novel kind of potential vorticity (PV), which collects together the relevant hydrodynamic and suspended sediment characteristics in a compact form. The semiquantitative result was that low-PV systems are associated with diffuse jets and mouth bar deposition, conditions associated with bifurcating channels, and a radial growth plan; high-PV jets exhibit little spreading, a condition that suppresses deposition at the center of the jet, thus leading to elongate channels. Although such an approach is derived from the Navier-Stokes and continuity equations, coupled with sediment mass conservation equation, it still represents only a primarily qualitative tool: It associates river outflow properties (i.e., sediment-PV) with channel morphology without providing a mechanistic relationship between flow characteristics and depositional patterns. Here we generalize and expand on that initial theory by investigating the physical relation between the flow vorticity structure and the suspended sediment distribution within a jet. In light of these new findings, we then analyze and discuss experimental data for a shallow wall-bounded plane jet.

[5] Depositional processes of sediment-laden turbulent jets should also account for unsteady properties [Rogerson *et al.*, 1999]: Shear instability at the jet boundaries creates unsteady coherent structures that were recently found to be related to lateral levee formation [Rowland *et al.*, 2009; Mariotti *et al.*, 2013]. Our approach only refers to the stationary component of the flow field, neglecting the presence of the large unsteady eddies and thus not differentiating between stable (no large eddies) and unstable (large eddies) jets. However, we provide a robust analytic framework that explains, mechanistically, the ability of a stationary jet to deliver sediment along the jet margins—a useful tool for describing long-term processes that create elongated levees.

2. The Sediment-PV Model

[6] A general framework for describing a sediment-laden river outflow (Figure 1) can be given by a novel application of the Ertel PV theorem [Ertel, 1942; Pedlosky, 1987; FJ10] in the following:

$$\frac{d\Pi_c}{dt} = \varepsilon_1 + \varepsilon_2, \quad (1)$$

where $\Pi_c \equiv \vec{\omega} / \rho \cdot \nabla c$ is an ad hoc PV that accounts for suspended sediment concentration (SSC, hereafter), $c(x, y, z, t)$, within the jet [FJ10]; $\vec{\omega}(x, y, z, t) = \nabla \times \vec{u}$ is the outflow relative vorticity (here planetary vorticity is neglected), which physically describes—in a local point of view—the internal rotation of the river outflow (Figure 1), whose velocity is $\vec{u} = (u, v, w)$; and ρ is the water density. The two terms in (1) are

$$\varepsilon_1 = \frac{\vec{\omega}}{\rho} \cdot \nabla \frac{dc}{dt}; \varepsilon_2 = \frac{\nabla c}{\rho} \cdot \left[\nabla \times \left(\frac{\vec{F}}{\rho} \right) \right], \quad (2)$$

where ε_1 is the sediment concentration change term since dc/dt can be expressed as sediment erosion and deposition functions [Parker, 1978; FJ10]; ε_2 is a frictional term: If, for instance, the external resistive force in (2) is taken as $\vec{F} = -(k/d) |\vec{u}| \vec{u}$, where $\vec{u} \approx (u, v, 0)$, d is the flow depth, and K is a dimensionless friction coefficient [Rowland *et al.*, 2009], then $\varepsilon_2 \approx -2(k/d)u\Pi_c$ for $u \gg v$ [FJ10]. We stress that, in its general form, ε_2 also accounts for lateral water entrainment effects (see section 3), which cause a PV evolution ($d\Pi_c/dt \neq 0$), resulting in a “flat” Gaussian shape of the horizontal velocity profile [FJ10].

[7] The new application of the Ertel theorem presented in (1) and (2) describes the Lagrangian evolution of sediment-PV, where ε_1 and ε_2 represent source/sink terms of PV. It is useful to remark that PV, in general, is not an absolute property of the flow: In the Ertel [1942] formulation, one can choose to set the PV by considering “some scalar fluid property λ ” that can be written as $\frac{d\lambda}{dt} = \Psi$ [Pedlosky, 1987]. Therefore, an ad

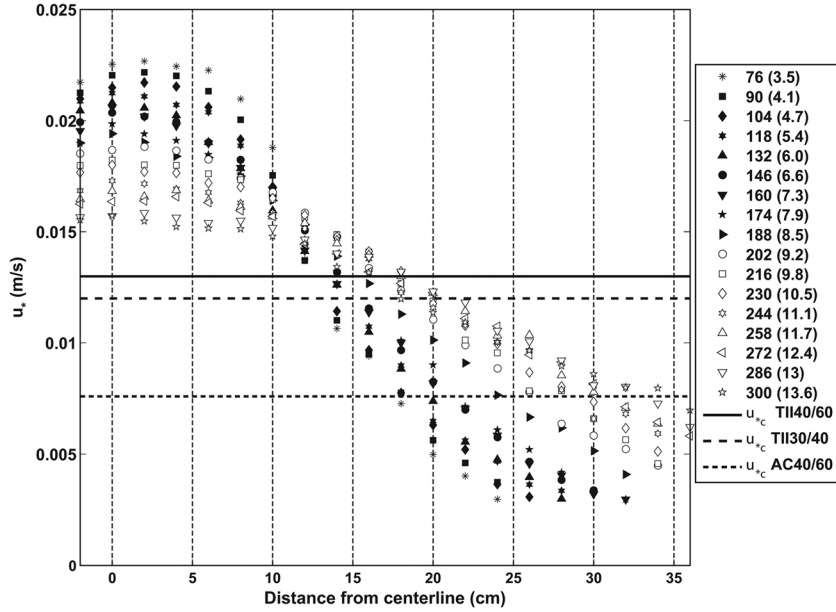


Figure 2. Shear velocities (u_*) calculated using depth-weighted mean velocities from *Rowland et al.*'s [2009] experimental data. The data are plotted by cross section with distance from the channel outlet indicated in centimeter and normalized by the outlet width (numerical values and values in parenthesis, respectively, in the box). The solid symbols are for sections within the transitional low-mixing rate zone, and the open ones are within the Zone of Established Flow, where the mean jet properties are consistent with prior experimental results on plane jets. The horizontal lines indicate the critical shear velocities needed to entrain the respective sediment types into suspension: AC40/60 (median grain size=0.41 mm; median settling velocity = 1.0 cm/s) is acrylic sediment with a specific gravity of 1.2; the TII40/60 (median grain size=0.48 mm; median settling velocity = 1.9 cm/s) and TII30/40 (median grain size=0.38 mm; median settling velocity = 2.6 cm/s) are Type II Urea sediment with a specific gravity of 1.5.

hoc PV (i.e., the sediment-PV in our case, where $\lambda = c$) provides some constraint on the vorticity, to the extent that the sediment can be considered a tracer, which generally becomes true as the Rouse number becomes small. In this sense, the PV view of suspended sediment dynamics can be seen as an alternative, complementary view of the traditional Rousean model in which the sediment concentration profile represents the balance between settling and turbulent mixing. This means that the self-organization of the flow in terms of velocity and SSC gradients can be modified by entrainment and loss of sediment (ε_1) as well as dissipative forces (ε_2). From this framework and by assuming that (i) an exchange of sediment between the jet and the boundaries does not affect the jet dynamics ($\varepsilon_1 \approx 0$) and (ii) the main vorticity component is the vertical one (i.e., $\vec{\omega} = (0, 0, \zeta)$, where $\zeta = \partial v / \partial x - \partial u / \partial y$), FJ10 proposed an analytic solution of equation (1), in a steady state, where PV exponentially decreases downstream due to friction, with a decay rate $2K/d \equiv L^{-1}$. Therefore, within a length scale $L^* < L/3$, the stationary component of the flow maintains its PV structure: The lateral shearing and the vertical SSC gradient are approximately uniform along the flow. Such a “constant-PV” zone has been identified as a region that would include both the “Zone Of Flow Establishment” (ZOFE, where jet centerline velocity is fairly constant downstream) and a transitional zone between the ZOFE and the “Zone Of Established Flow” (ZOEF, where the jet centerline velocity decays in a self-similar manner due to lateral mixing and friction) [Bates, 1953; Rowland et al., 2009]. Therefore, L^* would

mark the beginning of the ZOEF, where sediment-PV would no longer be conserved because of large lateral mixing and frictional effects [FJ10].

[8] Here we propose a modification to the general definition of PV that provides a more complete coupling between the hydrodynamic structure of a steady river jet and its SSC distribution:

$$\Pi_c \equiv \frac{\vec{\omega}}{\rho} \cdot \nabla c = \frac{1}{\rho} \left(\frac{\partial u}{\partial z} \frac{\partial c}{\partial y} + \zeta \frac{\partial c}{\partial z} \right), \quad \text{for } \vec{u} \approx (u, v, 0). \quad (3)$$

[9] This differs from the original FJ10 approach, where ζ was the only vorticity component, neglecting $(\partial u / \partial z)(\partial c / \partial y)$ and thus the vorticity effect due to bottom friction and the lateral SSC gradient. As we will show in section 4, such an expansion is of crucial importance if one seeks to couple hydrodynamics with suspended sediment theories.

[10] Although vertical velocity is not considered in (3), this general formulation includes vertical shearing (i.e., $\partial u / \partial z \neq 0$) and can therefore be considered a 2.5-dimensional model. In this regard, we remark that equation (3) holds for a jet velocity and SSC distribution that allow for, at least, the first derivative along y and z . The jet must show vertical and lateral shearing in the SSC, as well as vertical and lateral SSC stratification. We also note that by neglecting vertical velocities and the vertical gradient of the cross-stream velocity ($w = 0$ and $\partial v / \partial z = 0$), our definition of equation (3) does not take into account secondary circulations of the flow,

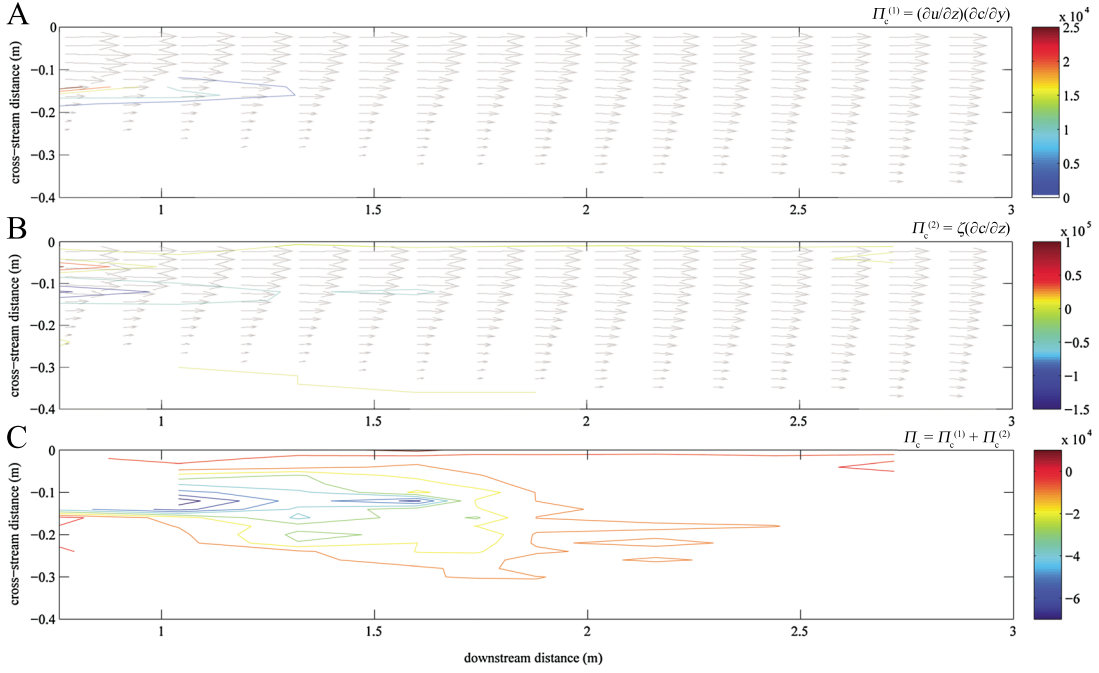


Figure 3. (a–c) PV contours [kg/s/m^4] as calculated from *Rowland et al.*’s [2009] experimental data for half of the sediment-laden jet (0 m in the cross-stream direction corresponds to the center line of the jet): Figures 3a and 3b are the potential vorticity contributions due to vertical ($\Pi_c^{(1)}$) and horizontal ($\Pi_c^{(2)}$) shearing, respectively; the horizontal, time- and depth-averaged velocity field (blue arrows) is superimposed in both panels (maximum velocity = 50 cm/s); Figure 3c is the total PV ($\Pi_c = \Pi_c^{(1)} + \Pi_c^{(2)}$); negative PV values indicate a clockwise rotation of the fluid from the centerline out toward the margin. The flow field was measured before the formation of the levee.

i.e., $\vec{\omega} = (0, \psi, \zeta)$, where $\zeta = \partial v/\partial x - \partial u/\partial y$ and $\psi = \partial u/\partial z$ (Figure 1). These assumptions may not be valid for channelized flows (in particular, if meanders are present), but they were experimentally found to hold for shallow wall-bounded plane jets [*Rowland et al.*, 2009].

[11] From 3, Π_c is now given by two main components (Figure 1):

$$\rho\Pi_c^{(1)} = \widetilde{\Pi_c^{(1)}} = \frac{\partial u}{\partial z} \frac{\partial c}{\partial y} \quad (4)$$

and

$$\rho\Pi_c^{(2)} = \widetilde{\Pi_c^{(2)}} = \zeta \frac{\partial c}{\partial z}, \quad (5)$$

where the tilde indicates the so called ‘‘PV substance’’, which has the physical properties of an actual tracer [*Haynes and McIntyre*, 1990]. We hereafter refer to PV substance only, neglecting the tilde.

[12] According to equation (4), $\Pi_c^{(1)}$ describes the coupling between vertical shear (Figure 1) due to bottom friction that acts to maintain sediment in suspension and the lateral distribution of SSC ($\partial c/\partial y$). In (5), $\Pi_c^{(2)}$ takes into account the horizontal velocity profile (Figure 1), i.e., lateral shearing $\partial u/\partial y$ and spreading $\partial v/\partial x$ of the jet (i.e., lateral momentum transport associated with lateral water entrainment), coupled with the vertical distribution of SSC ($\partial c/\partial z \neq 0$) is a necessary condition for the full 2.5-D PV definition in equation (3) and

will turn to be crucial in section 4. We remark that such a PV framework (Figure 1) describes the stationary component of the flow field, neglecting the explicit presence of large unsteady eddies [*Rogerson et al.*, 1999; *Rowland et al.*, 2009; *Mariotti et al.*, 2013].

[13] A direct, physical meaning of the Π_c in terms of sediment deposition is therefore provided by the following consideration. The cross-stream profile of the jet shear stress reflects the cross-stream profile of the downstream velocity [*Rowland et al.*, 2009]. A necessary condition for avoiding frontal deposition from suspension—assuming that the flow is under capacity—is that the shear stress (u^*) at the centerline of the outflow exceed the critical shear stress (u_c^*) required to suspend sediment (Figure 2) [*Rowland et al.*, 2010]. Therefore, if initially $u^* > u_c^*$ at the jet centerline, then the downstream evolution of $\zeta = \partial v/\partial x - \partial u/\partial y \approx -\partial u/\partial y$ (and thus of $\Pi_c^{(2)}$) describes the ability of the jet to maintain a critical difference in shear stress between its centerline and its lateral margins (Figures 1 and 2). For a high (low) ζ , one can expect a pronounced (flat) lateral shear stress profile. It is therefore clear that ζ gives some indication of sediment transport or deposition across the jet, consequently exerting a control on spatial depositional patterns, since levees develop in regions where $u^* < u_c^*$ [*Rowland et al.*, 2010]. We stress that ζ is here reasonably used as a proxy for $\partial u/\partial y$ (Figure 1) since the transverse velocities (v) are usually 2–3 orders of magnitude smaller than those of the downstream velocities (u) while $O(x) \approx 10O(y)$ [*Rowland*, 2007; *Rowland et al.*, 2009].

[14] From equations (4) and (5), one can therefore conclude that elongate levee deposition is characterized by two related

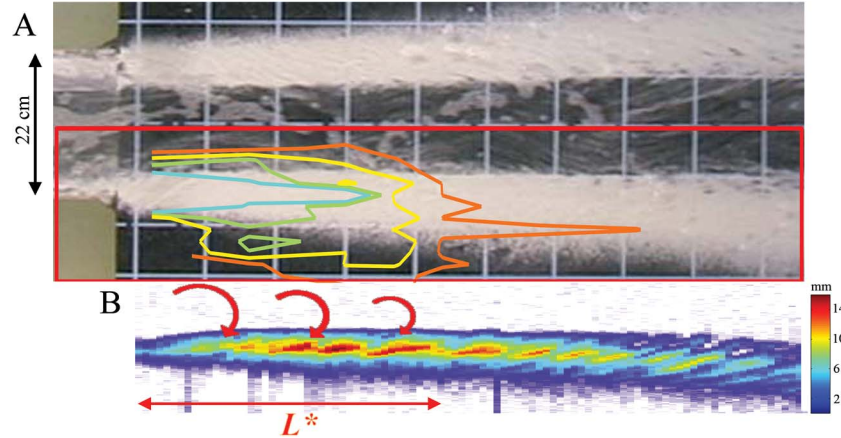


Figure 4. (a) Photographs at 2 min of a 20 min run showing the progressive development of levees [after Rowland *et al.*, 2010] (see Appendix A); each blue square is 20 cm by 20 cm and the transition from the gray entrance channel to the black, gridded bed occurs at 100 cm from the channel outlet; flow is from left to right; PV contour of Figure 3c is also superimposed. (b) Digital topography of the levee in the red box of Figure 4a; L^* represents the length over which PV is approximately conserved and over which mouth bar deposition is suppressed while levee building is predominant (see text); curling arrows represent the lateral advection/diffusion of suspended sediment. The red box in Figure 4a shows the area of Figure 4b.

processes: (1) a high $\Pi_c^{(1)}$ that indicates a high shear stress (i.e., suspended load conditions) and (2) a high $\Pi_c^{(2)}$ (i.e., higher shear stress at the central portion of the jet) that indicates $u^* > u_c^*$ at the jet centerline. Moreover, since c in (4) and (5) refers to suspended load, grain size is therefore a fundamental control factor: A dominantly coarse-grained efflux will lead to a low PV and thus to a frontal deposition. In the bed load limit, $c \rightarrow 0$ so that both PV terms vanish, and deposition is purely frontal (i.e., mouth bar).

3. Experimental Results

[15] To test our PV approach, we used high-resolution measurements of flow velocity and SSC distribution in a turbulent, sediment-laden jet, collected by Rowland *et al.* [2009, 2010] from a set of laboratory experiments (Appendix A) examining subaqueous levee formation downstream of a river mouth. Their results indicated that the rate of levee aggradation was dependent upon the rate of lateral dispersive flux of sediment toward the channel margins and also suspended sediment settling velocity [Rowland, 2007; Rowland *et al.*, 2009]. These experiments generated focused levee deposition and negligible mouth bar aggradation, providing us the opportunity to calculate each individual term of equation (3) for flow conditions known to produce an elongate channel morphology (Figure 3). We stress that the flow field was measured before the formation of the levee.

[16] Our diagnostic analysis, performed by considering time-averaged properties of the jet, shows that both sediment-PV terms $\Pi_c^{(1)}$ and $\Pi_c^{(2)}$ are comparable in magnitude (Figure 3): Lateral and vertical shearing, as well as lateral and vertical SSC gradients, described by (4) and (5), both play significant roles in the jet dynamics, suggesting an interplay between stationary flow vorticities and SSC profiles.

[17] In detail, both $\Pi_c^{(1)}$ and $\Pi_c^{(2)}$ show a peak at about $y \sim -0.12$ m cross stream (Figures 3a and 3b), which is the approximate location of the channel margin at the outlet, as

the channel mouth was 22 cm wide. These PV peaks mark the maximum lateral gradient of both horizontal velocity and SSC stationary profiles, revealing that the horizontal velocity profile, captured by ζ , affects the lateral SSC distribution, namely $\partial c / \partial y$, as experimentally noted by Rowland *et al.* [2009]. We also point out that the cross-stream distance $y \sim -0.12$ m can be recognized in the downstream evolution of the lateral shear stress profile (Figure 2): While the shear stress tends to decrease at the centerline and increase at the lateral margins of the outflow, it remains relatively constant at $y \sim -0.12$ m, as noted by Rowland *et al.* [2010]. As we will show later, this suggests that the portion of the flow where ζ (and thus Π_c) is maximum maintains its hydrodynamic characteristics, revealing some PV conservation property for that flow region. The memory of the channel width is therefore maintained as long as PV sink and source terms balance each other, and the dissipative effects do not modify the internal structure of the sediment-laden jet.

[18] The total PV (Figure 3c) appears to be maintained for about 1.8–1.9 m downstream before it fully decays. This distance marks the passage between a transitional low-mixing rate zone and the Zone of Established Flow (ZOEF), where turbulence generated by shearing along the margins of the jet penetrates to the jet core [Bates, 1953; Rowland *et al.*, 2009]. As we expect from the assumptions that used to define equation (3), sediment-PV cannot be maintained in the ZOEF because of the weak vertical and lateral shearing of the velocity field, as well as the lack of horizontal SSC gradient [Rowland, 2007].

[19] Figure 4a shows the spatial correlation between the sediment-PV structure of the experimental flow and its depositional pattern: Most of the levee deposition occurs within the high, constant PV zone, where the relation between flow vorticity and lateral advection/diffusion of sediment should reach its maximum. The existence of such a condition is also confirmed by the fact that the highest vertical aggradation of levees occurs where the conserved PV is the highest (Figure 4b).

[20] An interesting aside, we note that the sediment-PV decay observed from experimental data in the ZOEF (Figures 3 and 4)

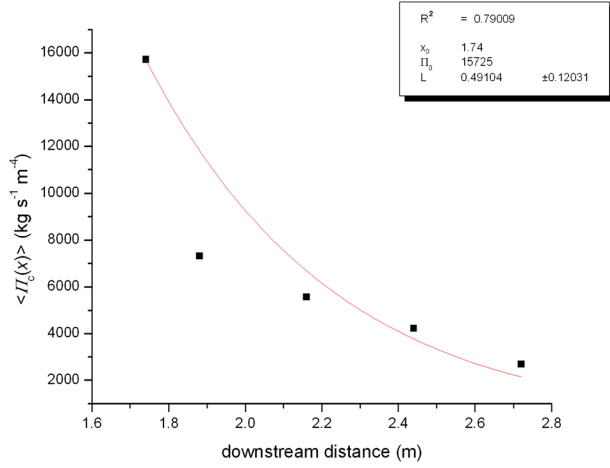


Figure 5. Downstream decay of cross-sectional averaged PV from experimental data (black squares) (details in Figure 3). Analytic solution of equation (1) for $\varepsilon_1 = 0$, namely $\langle \Pi_c(x) \rangle = \langle \Pi_c \rangle_0 \exp(-2 \frac{E+K}{d} x)$, where the decay rate coefficient $2 \frac{E+K}{d} = L^{-1}$ and $\langle \Pi_c(x) \rangle = \frac{1}{W/2} \int_0^{W/2} \Pi_c(x, y) dy$, where W is ~ 22 cm (line). A best fit as based on this analytic result gives $L \sim 0.5$ m, which gives a friction coefficient $K \sim O(10^{-3})$, where $d = 0.05$ m and $E \sim O(10^{-2})$ [Wang, 1984]. Since there were no available velocity—and thus PV—data from 0 to 1 m, we assumed a constant PV (i.e., $\Pi_0 \sim 15000 \text{ kg s}^{-1} \text{ m}^{-4}$) for that region, in accordance with Figure 3c. Therefore, the exponential fit starts from the ZOEf (i.e., $x \sim 1.8$ m).

can be used to estimate the bottom friction coefficient K . We fit an exponential decay of the cross section-averaged experimental PV, namely $\frac{1}{W/2} \int_0^{W/2} \Pi_c(x, y) dy = \langle \Pi_c(x) \rangle$ (where W is the cross-stream length), suggested by an analytic solution of equation 1 for $\varepsilon_1 = 0$ and $\varepsilon_2 \approx -\frac{2(E+K)}{\rho} u \langle \Pi_c(x) \rangle$. This is similar to the approximation proposed by FJ10 and shown in section 2; however, such a ε_2 also includes the frictional effects due to lateral mixing, parameterized by the entrainment coefficient $E \sim O(10^{-2})$ [Ellison and Turner, 1959; Wang, 1984]. By comparing the theoretical decay, i.e., $\langle \Pi_c(x) \rangle = \langle \Pi_c \rangle_0 \exp(-2 \frac{E+K}{d} x)$, with the experimental one ($\langle \Pi_c(x) \rangle = \langle \Pi_c \rangle_{x=1.75} \exp(-x/L)$) starting from the ZOEf, we obtain a friction coefficient, $K \sim O(10^{-3})$ (Figure 5). We remark that the FJ10 analytic solution for equation (1) does not capture the initial constancy of PV, and therefore, the regression coefficient R^2 cannot be expected to be close to unity (Figure 5). However, the friction coefficient we obtain is well within the range found in the literature and agrees reasonably well with the drag coefficient, $C_d \sim 1.6 \times 10^{-3}$, estimated by Rowland *et al.* [2010] using high-resolution shear stress measurements.

[21] Results from this section, and in particular the recognized spatial sediment-PV distribution and its correlation with the depositional pattern, will be used later on for validating new theoretical developments regarding flow vorticity and sedimentary properties of the jet.

4. Sediment-PV and Suspension in a Shear Flow

[22] Our results suggest that $\Pi_c \approx \bar{\Pi}_c = \text{const}$ along a region where sediment-PV source/sink terms either compensate for

each other or are not significant (see equation (1)). Here we pair constant sediment-PV with the Rouse [1937] theory for suspension in a shear flow to investigate the relation between stationary flow vorticity and lateral sediment diffusion/advection. From this coupling, we expect to find some insights on the mechanistic processes that forms elongated channels.

[23] In a turbulent boundary layer flow, the equilibrium SSC profile results from a balance of the two vertical fluxes of sediment [Rouse, 1937]

$$v_s c + k_{sed}^z \frac{\partial c}{\partial z} = 0, \quad (6)$$

where v_s is the hindered sediment settling velocity and k_{sed}^z is the vertical sediment eddy diffusivity coefficient. Relating k_{sed}^z to the vertical diffusivity coefficient of the momentum (i.e., the kinematic viscosity) and assuming a linear relation for the boundary shear stress (see Appendix B), we obtain from (6) a proportionality relation between vertical shear velocity and vertical SSC gradient (i.e., $\partial u / \partial z \propto \partial c / \partial z$). For $(\partial u / \partial z)(\partial c / \partial y) + \zeta(\partial c / \partial z) \approx \bar{\Pi}_c$, we therefore obtain a relation that pairs ζ with $\partial c / \partial y$ (Figure 6; see Appendix B) in the following:

$$\frac{\partial c}{\partial y} = \frac{\bar{\Pi}_c d}{\alpha y(d-z)} + \frac{cd}{\gamma(d-z)}, \quad (7)$$

where $\alpha = -\partial \ln c / \partial z$, $\gamma = \tau_0 / (\rho v_s)$, and τ_0 is the boundary shear stress. It is worth noting that $\partial c / \partial y$ in (7) is also modulated by the water depth and the SSC.

[24] Equation (7) can be therefore used in a general formulation for advection and lateral diffusion of sediment [Parker *et al.*, 1986; Van Rijn, 1986], namely

$$\frac{\partial c}{\partial t} + \frac{\partial uc}{\partial x} + \frac{\partial vc}{\partial y} = \frac{\partial}{\partial y} \left(k_{sed}^y \frac{\partial c}{\partial y} \right) - \left(v_s \frac{\partial c}{\partial z} \right), \quad (8)$$

where for the sake of simplicity, we assume net depositional conditions by neglecting the flux of sediment resuspended from the bed. With the aid of (7), equation (8) gives the total deposition rate (D_{tot}) in steady state

$$\begin{aligned} D_{tot} &= \int_0^d \left(\frac{\partial}{\partial y} \left(k_{sed}^y \frac{\partial c}{\partial y} \right) - \frac{\partial uc}{\partial x} - \frac{\partial vc}{\partial y} \right) dz \\ &\propto \int_0^d k_{sed}^y \Gamma(z) \left[c \frac{\partial \zeta}{\partial y} + \left(\frac{\bar{\Pi}_c}{\alpha} + c \zeta \right) \left(\Gamma(z) \zeta - \frac{v}{k_{sed}^y} \right) \right] dz, \end{aligned} \quad (9)$$

where $\Gamma(z) = \frac{d}{\gamma(d-z)}$.

[25] The integral (9) is performed at each (x, y) point of the jet ($D_{tot} = D_{tot}(x, y)$) and is valid for $\Pi_c \approx \bar{\Pi}_c = \text{const}$ (Figure 3c). By merely considering the stationary component of the flow, equation (9) explains how levee deposition due to lateral diffusion/advection of sediment is directly related to ζ within a low-mixing rate zone where sediment-PV is conserved. Total deposition will be large where both vorticity and cross-stream vorticity gradient are large. This theoretical result agrees with our experimental findings (section 3): The experimental jet, indeed, shows a PV peak at about $y \sim -0.12$ m (Figures 3a and 3b), which corresponds to the cross-stream distance where levee deposition occurs (Figure 4). One can moreover note the quadratic term $c \Gamma(z) \zeta^2$ in (9), which plays a crucial role in very high vorticity systems where the

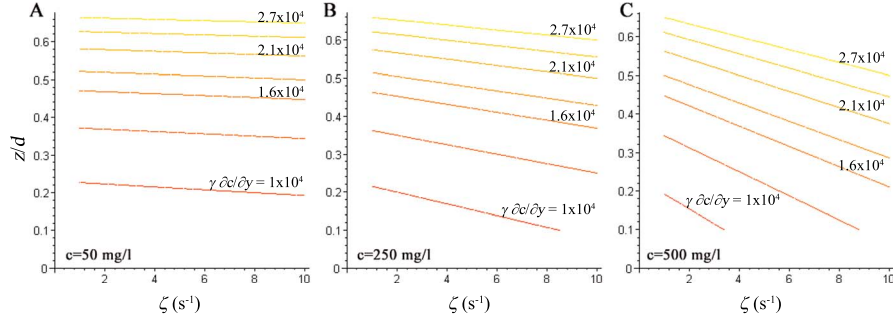


Figure 6. Contour plot of $\gamma\partial c/\partial y$ from equation (7) as a function of the vertical vorticity component, ζ , and the normalized depth z/d , for different suspended sediment concentration (SSC): (a) $c = 50$ mg/L, (b) 250 mg/L, and (c) 500 mg/L. Note how the proportionality between ζ and $\gamma\partial c/\partial y$ is strongly affected by the local SSC: At a given depth, for large (small) sediment in suspension, variations of ζ correspond to large (small) variations of $\gamma\partial c/\partial y$. The proportionality depends only weakly on depth.

mean horizontal velocity over the width of the channel outlet, i.e., U/W , is greater than 1 s^{-1} . According to (7) and (9), levee deposition is also tuned by the SSC and increases with distance z above the bed (Figure 6), justifying the ability of high-PV jets to form levees, where the sediment must come from the upper portion of the water column.

5. Discussion

5.1. Physical Meanings of Sediment-PV Conservation

[26] The coupling between sediment-PV and the Rouse profile (6) leads to the following physical analysis. If conserved, PV tells us that variations of ζ must be followed by variations of $\partial c/\partial z$ (equation (5)): Stretching the vertical vortex tube (Figure 1) increases δz (i.e., $\partial c/\partial z$ decreases), and thus, ζ must increase (a similar discussion can start from equation (4)). For equation (6) however, variations of $\partial c/\partial z$ bring the system to a new state where the sediment in suspension is no longer in equilibrium with the vertical shear of the flow ($\partial u/\partial z$). Hence, this would cause either an upward or downward movement of sediments, such that sediment-PV is not conserved. In order that $\Pi_c \approx \text{const}$, both the Rouse profile and the lateral shear must remain unvaried in the streamwise direction. This case, along with equation (9), shows that elongated levee deposition requires two main conditions: (i) a high PV at the river mouth that triggers a lateral diffusion/advection mechanism for the sediment as described in (7) and (9) and (ii) small spatial PV variation—caused by a balance between frictional forces and sediment loss—to maintain the jet structure. In other words, elongated levees would form if the loss in transport capacity is smaller than the loss of transported sediments. The onset of the PV sources described in (2) would therefore break such a constraint for flow vorticity and thus the mechanistic relation that connects vorticity to lateral sedimentation.

[27] Sediment-PV conservation requires mild or negligible spreading of the jet along the low-mixing rate zone. In steady state,

$$\frac{d\Pi_c}{dt} = \vec{u} \cdot \nabla \Pi_c = 0, \quad (10)$$

which indicates that the flow velocity \vec{u} must be orthogonal to the PV gradient: \vec{u} cannot cross the surfaces where

$\Pi_c = \text{const}$. For our experimental analysis, iso-PV surfaces (Figure 3) tend to be parallel to the downstream direction of the flow, and thus, jet spreading remains weak within the low-mixing rate zone. This feature is in agreement with the self-sharpening property of PV-conserved stationary jets [Wood and McIntyre, 2010]. Equation (10) is also plotted for the experimental data and, as we expected, is verified for a distance $x \sim 1.5$ m (Figures 3 and 7). Yet if PV source/sink terms are no longer negligible, flow velocities would penetrate the iso-PV surfaces, giving rise to a more diffusive behavior (i.e., spreading) of the jet that might trigger frontal bar deposition.

[28] The mechanistic process for levee building (i.e., equation (9)) that is derived from the sediment-PV conservation here discussed cannot be extended to the ZOEf, where lateral and vertical gradients of velocity and SSC are no longer well defined. This might suggest that (i) the formation of levees moves the outlet mouth forward and hence extends the ZOEf, (ii) the deposit that formed within the low-mixing zone modifies the flow field and moves the jet outlet forward, or (iii) levee formation with the ZOEf needs to be explained by the presence of unsteady coherent structures, such as large eddies [Mariotti et al., 2013]. We believe that, for the ZOEf, the latter approach proposed by Mariotti et al. [2013] is currently providing the most reasonable explanation for levee formation in this highly turbulent zone and is complementing our work.

5.2. Further Implication of Sediment-PV Conservation in a Sediment-Laden Jet

[29] As we mentioned above, sediment-PV conservation can be due to the balance between the frictional and sediment concentration change terms, that is, $d\Pi_c/dt = \varepsilon_1 + \varepsilon_2 = 0 \rightarrow \varepsilon_1 = -\varepsilon_2$. This implies that while PV would naturally decrease because of the divergence of sediment loss ($\varepsilon_1 < 0$), vertical and lateral shearing of the flow due to friction would counteract the settling process by playing the role of a PV source ($\varepsilon_2 > 0$). From 2, this balance gives

$$\vec{\omega} \cdot \nabla \frac{dc}{dt} = -\nabla c \cdot \left[\nabla \times \left(\frac{\vec{F}}{\rho} \right) \right], \quad (11)$$

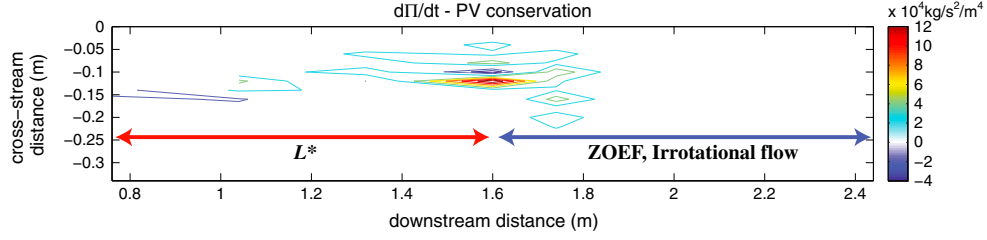


Figure 7. Test for steady state PV conservation by plotting $\vec{u} \cdot \nabla \Pi_c$ from Rowland *et al.*'s [2009] experimental data. As for Figure 4, L^* represents the length scale over which PV $\neq 0$ is approximately conserved, over which mouth bar deposition is suppressed while levee building is predominant (see text). After a strong PV variation at $x \sim 1.6$ m, the downstream zone, which corresponds to the ZOEf in Rowland *et al.* [2009], is found to be irrotational (i.e., $|\vec{\omega}| \approx 0$).

and by using, for instance, the friction form $\vec{F} = \frac{-K}{d} |\vec{u}| \vec{u}$ [FJ10] and the sediment conservation equation [Edmonds and Slingerland, 2007]

$$\frac{dc}{dt} = v_s \frac{\partial c}{\partial z} + \frac{\partial}{\partial x} \left(k_{\text{sed}}^x \frac{\partial c}{\partial x} \right) + \frac{\partial}{\partial y} \left(k_{\text{sed}}^y \frac{\partial c}{\partial y} \right) + \frac{\partial}{\partial z} \left(k_{\text{sed}}^z \frac{\partial c}{\partial z} \right), \quad (12)$$

after some cumbersome algebra, we arrive at

$$\begin{aligned} \vec{\omega} \cdot \nabla \left[v_s \frac{\partial c}{\partial z} + \frac{\partial}{\partial y} \left(k_{\text{sed}}^y \frac{\partial c}{\partial y} \right) + \frac{\partial}{\partial z} \left(k_{\text{sed}}^z \frac{\partial c}{\partial z} \right) \right] \\ = \left(\frac{-2k}{d} |\vec{u}| \right) \vec{\omega} \cdot \nabla c. \end{aligned} \quad (13)$$

[30] Hence, we obtain

$$\vec{\omega} \cdot \nabla \wp = 0, \quad (14)$$

where

$$\wp = \left[v_s \frac{\partial c}{\partial z} + \frac{\partial}{\partial y} \left(k_{\text{sed}}^y \frac{\partial c}{\partial y} \right) + \frac{\partial}{\partial z} \left(k_{\text{sed}}^z \frac{\partial c}{\partial z} \right) + \left(\frac{2k}{d} |\vec{u}| \right) c \right]. \quad (15)$$

[31] We can now consider the sufficient conditions for sediment-PV conservation by finding three different cases where equation (14) is satisfied:

[32] 1. the fluid is irrotational, i.e., $\vec{\omega} = 0$,

[33] 2. $\vec{\omega} \perp \nabla \wp = 0$

[34] 3. $\wp = \left[v_s \frac{\partial c}{\partial z} + \frac{\partial}{\partial y} \left(k_{\text{sed}}^y \frac{\partial c}{\partial y} \right) + \frac{\partial}{\partial z} \left(k_{\text{sed}}^z \frac{\partial c}{\partial z} \right) + \left(\frac{2k}{d} |\vec{u}| \right) c \right] = 0$

[35] Each of these cases finds an interesting physical interpretation. In the first case, sediment-PV is not only conserved but also identically null. The experimental results show that this particular condition occurs along the ZOEf (Figures 3 to 7), where PV constancy corresponds to a negligible vorticity field (i.e., irrotational flow).

[36] The case (ii) is related to the physical and geometrical meaning of the scalar field \wp . By neglecting the term due to bottom drag and concentrating on the vertical distribution of

sediments, \wp is the divergence of the sediment flux; according to Fick's law,

$$\wp = \frac{\partial}{\partial z} \left(v_s c + k_{\text{sed}}^z \frac{\partial c}{\partial z} \right) = \nabla \cdot J, \quad (16)$$

where

$$J(z) = \left(v_s c + k_{\text{sed}}^z \frac{\partial c}{\partial z} \right) \quad (17a)$$

is the rate at which sediment is vertically transported through a unit area. If the net vertical transport is equal to zero, equation (18) coincides with the Rouse [1937] equilibrium (see equation (6)). In a more general 2-dimensional case, equation (18) is

$$J(y, z) = \left(v_s c + \vec{k} \cdot \nabla c \right), \quad \text{where } \vec{k} = (0, k_{\text{sed}}^y, k_{\text{sed}}^z). \quad (17b)$$

[37] In this view (by means of either (17a) or (17b)), condition (ii) can be stated as the following: sediment-PV is conserved if the vorticity vector is purely orthogonal to the vector gradient of the divergence of the flux of sediments. In its classical formulation, the Rouse profile can be seen as a vortex tube oriented along the y axis that generates SSC gradients oriented along z ; the condition $\vec{\omega} \perp \nabla \wp = 0$, and thus 19, is therefore generalizing this view in a 2-D space, defined by the (y, z) plane, by taking into account both SSC gradients along y and z .

[38] Case (iii) gives a relation between SSC distribution and shearing velocities. For $\wp = 0$, we have

$$v_s \frac{\partial c}{\partial z} + \frac{\partial}{\partial y} \left(k_{\text{sed}}^y \frac{\partial c}{\partial y} \right) + \frac{\partial}{\partial z} \left(k_{\text{sed}}^z \frac{\partial c}{\partial z} \right) + \left(\frac{2k}{d} |\vec{u}| \right) c = 0, \quad (18)$$

which, indeed, represents the balance between the divergence of the sediment flux $V(y, z)$ and the friction.

5.3. Physical Meanings of Sediment-PV for Fluvial Systems

[39] We finally provide a physical explanation of sediment-PV. By scaling the PV from equation (3), we find [FJ10]

$$\frac{\partial u}{\partial z} \frac{\partial c}{\partial y} + \zeta \frac{\partial c}{\partial z} \approx \frac{U}{d} \frac{C}{W} + \frac{U}{W} \frac{C}{d} = \frac{Q_s}{A^2}, \quad (19)$$

where $\zeta = \partial v/\partial x - \partial u/\partial y \approx -\partial u/\partial y$, as described in section 2 [Rowland *et al.*, 2009]. In (B2) U [L/T] and C [M/L³] are scale values for outflow velocity and SSC at the channel mouth, respectively; we then multiplied both denominator and numerator by Wd [L²], obtaining the suspended load sediment flux (i.e., $Q_s = UCWd$ [M/T]) through the channel outlet over the square of cross-sectional area of the channel (i.e., $A^2 = (Wd)^2$). According to (B2), a high-PV system would represent a river plume with a high suspended load sediment flux through a small cross-sectional area, a feature that agrees with the concept that a low-spreading jet, with a pronounced horizontal velocity profile at the river mouth, gives rise to elongate channels and suppresses vertical frontal bar aggradation.

[40] Let us stress that Q_s/A^2 does not “set” the actual sediment-PV of the jet, which is given by shear velocities and SSC gradients within the channelized flow; rather, such a scaling—beyond providing an intuitive way to describe PV—works as a bulk PV estimation when detailed measurements may not be available at and around the channel mouth. Indeed, by means of (B2), Falcini *et al.* [2012] monitored velocity and SSC (and thus PVs) of the Mississippi and Atchafalaya River plumes from remote sensing and in situ data (such as sea surface temperature, SSC estimations, and current meter data) and verified the PV constancy that characterized the low-spreading jet outflowing the Mississippi River southwest pass. In such a context, equation (B2) represents a semiquantitative tool for detecting those river plume systems that need to be “modified” in order to change their depositional behavior. However, such a morphological change can only be given by equations (1)–(3), that is, by directly acting on the shearing characteristics of the flow through any kind of tool that lowers the flow internal vorticities (i.e., ζ and ψ). This would give a PV-evolution that creates a different depositional pattern.

[41] Land-building proposals desire a radially growing delta that fills space to provide a land buffer. Kim *et al.* [2009a] have proposed that diversions must be deep in order to tap into coarser (sand) sediment that is concentrated in the bottom of the channel. The PV theory allows one to estimate the width of a diversion channel for a given sediment discharge in order to promote bifurcation and hence a radially growing delta.

6. Conclusions

[42] We propose and explore, both theoretically and experimentally, a PV-conservation approach to relate channel mouth depositional patterns to hydrodynamics and sediment transport characteristics of river mouths. Within a low mixing region, over which $\Pi_c \approx \text{const}$, we found a physically based relation between the internal flow vorticity and the advection/diffusion of sediment toward the lateral margins of the outflow. In this region, if sediment-PV is large, then levee deposition is the dominant river-mouth process, and a channel is expected to elongate by building self-confining levees. Bar deposition is also suppressed since the high vorticity indicates a high shear stress at the centerline. Low PV should encourage mouth bar deposition and bifurcation.

[43] The length scale defined by $\Pi_c \approx \text{const}$ —which seems to correspond to the initial low-mixing zone (i.e., ZOFE and

the transitional zone between ZOFE and ZOEF) where levee deposition occurs while mouth bar deposition is suppressed—is essentially a hydrodynamic length scale where the absolute sediment concentration and the lateral shear control the rates of levee deposition. Also, through the Rouse relation, we found that the SSC distribution is not independent of the flow and is therefore (at least partially) controlled by hydrodynamics as well.

[44] Our approach approximates the turbulent jet as a steady flow. It has been recently found that unsteady coherent structures (i.e., meanders with a horizontal scale $\sim W$ and time scale of $\sim W/U$) may be related to the formation of lateral levees [Rowland *et al.*, 2009]. From these observations, Mariotti *et al.* [2013] considered the coupling between the vertical dynamics of suspended sediment and the advection of such coherent structures. Their results show that lateral sediment deposition (i.e., deposition at the farthest distance from the jet centerline) occurs when the time scale for sediment settling (T_D) is close to the time scale for an eddy to perform one-half revolution ($T_E \propto W/U$). In other words, this tells us that rapid levee formation occurs when a decrease of T_D is followed by a decrease of T_E , which would correspond to high vorticity since $\zeta \sim U/W$. Interestingly, such a condition agrees with our steady PV theory, which does not need to resolve and take into account unsteady properties of the flow.

[45] Our PV formulation allows us to analytically probe the hydrodynamic processes that lead to the formation of various channel patterns. The derived linear relation between flow vorticity and lateral sediment transport provides a mechanistic foundation for the commonly observed correlation between the lateral diffusion and turbulent processes [Rowland *et al.*, 2010]. In sum, sediment-PV provides a compact formulation for combining two critical elements in suspended sediment dynamics: velocity shear and sediment concentration gradients for steady flows. This makes it especially useful for quantifying long time-averaged processes like levee deposition that depend on lateral sediment transfer. We indeed clarify, from theory, what the important variables for channel mouth depositional behaviour should be (i.e., internal shearing of the flow), explaining how and why some systems are more prone to build elongated channels at river mouths.

Appendix A: Experimental Setting and Numerical Analysis

[46] The data for our numerical analysis was obtained from experiments by Rowland *et al.* [2010]. The experiments were performed at the Richmond Field Station at U. C. Berkeley in an experimental basin measuring 8 m in length, 3 m in width, and 0.6 m in depth with an acrylic bed 2.4 m wide and 3.7 m long. Water was fed in through a constant head tank leading to a stilling box, to a flow straightener, and then through a 1 m long channel feeding into the basin. The channel walls were 4 cm high at the start of the channel and had a constant downward slope to 0 cm at the end of the channel, where 0 cm is defined as the height of the bed. The walls had an initial width of 22 cm and increased gradually to 25.5 cm at the channel outlet. For the experiments, the mean flow depth of the jet and basin was 5 cm [Rowland *et al.*, 2010].

[47] A Nortek Vectrino Acoustic Doppler Velocimeter (ADV) was used to take velocity measurements at five elevations within the flow to obtain vertical velocity profiles. Measurements were taken every 2 cm across half of the jet (from a point 2 cm across the centerline to the jet margin) and every 14 cm downstream. The measurements were obtained at heights of 0.8, 1.02, 1.32, 2.78, and 4.25 cm above the average bed elevation at a frequency of 25 Hz and over a period of 120 s [Rowland *et al.*, 2010].

[48] Experiments were also conducted by Rowland *et al.* [2010] using sediment to examine levee deposition, and suspended sediment concentration profiles were obtained from these experiments. Measurements of suspended sediment concentration (SSC) were taken for runs with a plastic sediment with a median grain size of 380 μm , a specific gravity of 1.5, and a median settling velocity of 1.9 cm/s. The SSC was abstracted from images taken using a 500 mW LasirisTM Magnum SP infrared laser and an EPIX, Inc. Silicon[®] 1281 high-speed video digital camera [Rowland, 2007]. The flow was imaged at a resolution of 0.138 mm per pixel over a width of 6 cm with a frame rate of 10 frames per second and a period of 1 min across the half-jet. Images were taken for ten cross sections at 76, 104, 132, 160, 174, 186, 216, 244, 272, and 300 cm downstream. Concentrations were determined by calculating the mean intensity for each pixel over the 1 min period, averaging them over an area of 2 cm in width by 0.4 cm in depth (thus creating a grid of data similar to that of the velocity data), and using an empirically determined intensity-sediment concentration calibration [Rowland *et al.*, 2010].

Appendix B: PV and Suspension in a Shear Flow

[49] We now obtain a linear relationship between ζ and $\partial c/\partial y$, starting from the Rouse [1937] theory and the conservation of PV, within the transitional zone where the condition of self-similar Gaussian velocity distributions has not developed [Albertson *et al.*, 1950; Rowland *et al.*, 2009].

[50] The Rouse [1937] formulation is used to obtain the vertical SSC profile. In a turbulent boundary layer flow, the equilibrium sediment concentration profile results from a balance of the two vertical fluxes of sediment:

$$v_s c + k_{\text{sed}}^z \frac{\partial c}{\partial z} = 0, \quad (\text{B1})$$

where v_s is the hindered sediment settling velocity and k_{sed}^z is the vertical sediment eddy diffusivity coefficient. The first and second term in B3 represent advective settling downward and upward directed turbulent diffusion, respectively. Assuming that $k_{\text{sed}}^z = \beta k^z$, where k^z is the vertical diffusivity coefficient of the momentum (i.e., the kinematic viscosity) and $\beta \sim 1$ is a proportionality coefficient, one can use the boundary shear stress

$$\tau = \rho k^z \frac{\partial u}{\partial z} \approx \tau_0 \left(1 - \frac{z}{d}\right) \quad (\text{B2})$$

together with (B3) to obtain

$$\frac{\partial u}{\partial z} = \varphi(z) \frac{\partial c}{\partial z}, \quad (\text{B3})$$

where $\varphi(z) = \frac{\tau_0(z-d)}{v_s \rho d}$, d is the flow depth, and τ_0 is boundary shear stress at the bottom.

[51] In addition, from the assumption of constant PV, one has

$$\frac{\partial u}{\partial z} \frac{\partial c}{\partial y} + \zeta \frac{\partial c}{\partial z} \approx \bar{\Pi}_c \quad (\text{B4})$$

which, with the aid (B5), gives

$$\varphi(z) \frac{\partial c}{\partial z} \frac{\partial c}{\partial y} + \zeta \frac{\partial c}{\partial z} = \bar{\Pi}_c. \quad (\text{B5})$$

[52] Recalling that $\frac{1}{f(x)} \frac{\partial f}{\partial x} = \frac{\partial \ln f}{\partial x}$ and by using the coefficient $\varphi(z)$, (B5) can be written as

$$\frac{\tau_0(z-d)}{v_s \rho d} \frac{\partial \ln c}{\partial z} \frac{\partial c}{\partial y} + \zeta c \frac{\partial \ln c}{\partial z} = \bar{\Pi}_c \quad (\text{B6})$$

where $\frac{\partial \ln c}{\partial z} \approx -\alpha$ can be considered constant, according to experimental results [Rowland *et al.*, 2010].

[53] This finally gives

$$\frac{\partial c}{\partial y} = \frac{\bar{\Pi}_c d}{\alpha \gamma (d-z)} + \frac{cd}{\gamma (d-z)} \zeta, \quad (\text{B7})$$

where $\gamma = \tau_0/\rho v_s$.

[54] **Acknowledgments.** We gratefully acknowledge the support by the National Science Foundation through contract EAR-0746138 to D.J.J., via the National Center for Earth-surface Dynamics (NCED), a Science and Technology Center funded under agreement EAR-0120914, and by FESD: A Delta Dynamics Collaboratory under agreement EAR-1135427 to C.P., via the Italian National Flag Project RITMARE (Marine Italian Research) funded by the Italian Ministry of Education, University and Research within the National Research Program 2011–2013 to FF. This work was inspired by discussions at the Doolin “deltas workshop” with A. Fowler, C. Stark, J. Swenson, and V. Voller, sponsored by the National Center for Earth-surface Dynamics.

References

- Abramovich, G. N. (1963), *Theory of Turbulent Jets*, 684 pp., MIT Press, Cambridge, Mass.
- Albertson, M. L., Y. B. Dai, R. A. Jensen, and H. Rouse (1950), Diffusion of submerged jets, *Trans. Am. Soc. Civ. Eng.*, *115*, 639–664.
- Bates, C. C. (1953), Rational theory of delta formation, *AAPG Bull.*, *37*(9), 2119–2162.
- Blum, M. D., and H. H. Roberts (2009), Drowning of the Mississippi Delta due to insufficient sediment supply and global sea-level rise, *Nat. Geosci.*, *2*, 488–491.
- Blum, M. D., and T. E. Tornqvist (2000), Fluvial responses to climate and sea-level change: A review and look forward, *Sedimentology*, *47*, 2–48.
- Day, J. W., L. D. Britsch, S. R. Hawes, G. P. Shaffer, D. J. Reed, and D. Cahoon (2000), Pattern and process of land loss in the Mississippi Delta: A Spatial and temporal analysis of wetland habitat change, *Estuaries Coasts*, *23*, 425–438.
- Edmonds, D. A., and R. L. Slingerland (2007), Mechanics of middle-ground bar formation: Implications for the morphodynamics of delta distributary networks, *J. Geophys. Res.*, *112*, F02034, doi:10.1029/2006JF000574.
- Edmonds, D. A., and R. L. Slingerland (2010), Significant effect of sediment cohesion on delta morphology, *Nat. Geosci.*, *3*, 105–109.
- Ellison, T. H., and J. S. Turner (1959), Turbulent entrainment in stratified flows, *J. Fluid Mech.*, *6*, 423–448.
- Ertel, H. (1942), Ein neuer hydrodynamischer Wirbelsatz, *Meteorol. Z.*, *59*(2), 277–281.
- Falcini, F., and D. J. Jerolmack (2010), A potential vorticity theory for the formation of elongate channels in river deltas and lakes, *J. Geophys. Res.*, *115*, F04038, doi:10.1029/2010JF001802.
- Falcini, F., et al. (2012), Linking the historic 2011 Mississippi River flood to coastal wetland sedimentation, *Nat. Geosci.*, *5*, 803–807.
- Haynes, P. H., and M. E. McIntyre (1990), On the conservation and the impermeability Theorems for Potential Vorticity, *J. Atmos. Sci.*, *47*, 2021–2031.

- Kim, W., D. Mohrig, R. Twilley, C. Paola, and G. Parker (2009a), Is it feasible to build new land in the Mississippi River Delta?, *Eos Trans. AGU*, 90(42), 373–374.
- Kim, W., A. Dai, T. Muto, and G. Parker (2009b), Delta progradation driven by an advancing sediment source: Coupled theory and experiment describing the evolution of elongated deltas, *Water Resour. Res.*, 45, W06428, doi:10.1029/2008WR007382.
- Kostic, S., and G. Parker (2003), Progradational sand-mud deltas in lakes and reservoirs. Part 1. Theory and numerical modeling, *J. Hydraul. Res.*, 41, 127–140.
- Mariotti, G., F. Falcini, N. Geleynse, M. Guala, T. Sun, and S. Fagherazzi (2013), Sediment eddy diffusivity in meandering turbulent jets: Implications for levee formation at river mouths, *J. Geophys. Res. Earth Surf.*, 118, 1908–1920, doi:10.1002/jgrf.20134.
- Nittrouer, C. A. (1999), Strataform: Overview of its design and synthesis of its results, *Mar. Geol.*, 154(1–4), 3–12.
- Paola, C. (2000), Quantitative models of sedimentary basin filling, *Sedimentology*, 47, 121–178.
- Paola, C., R. R. Twilley, D. A. Edmonds, G. Parker, E. Viparelli, and V. R. Voller (2011), Natural processes in delta restoration: Application to the Mississippi Delta, *Annu. Rev. Mar. Sci.*, 3, 67–91.
- Parker, G. (1978), Self-formed straight rivers with equilibrium banks and mobile bed. Part 1. The sand-silt river, *J. Fluid Mech.*, 89, 109–125.
- Parker, G., Y. Fukushima, and H. M. Pantin (1986), Self-accelerating turbidity currents, *J. Fluid Mech.*, 171, 145–181, doi:10.1017/S0022112086001404.
- Parker, G., C. Paola, K. X. Whipple, and D. C. Mohrig (1998), Alluvial fans formed by channelized fluvial and sheet flow. I: Theory, *J. Hydraul. Eng.*, 124, 985–995.
- Peckham, S. D. (2008), A new method for estimating suspended sediment concentrations and deposition rates from satellite imagery based on the physics of plumes, *Comput. Geosci.*, 34(10), 1198–1222.
- Pedlosky, J. (1987), *Geophysical Fluid Dynamics*, Springer, New York.
- Rajaratnam, N. (1976), *Turbulent Jets. Developments in Water Science*, Elsevier, Amsterdam.
- Rogerson, A. M., P. D. Miller, L. Pratt, and C. Jones (1999), Lagrangian motion and fluid exchange in a barotropic meandering jet, *J. Phys. Oceanogr.*, 29(10), 2635–2655.
- Rouse, H. (1937), Modern conceptions of the mechanics of turbulence, *Trans. Am. Soc. Civ. Eng.*, 102, 436–505.
- Rowland, J. C. (2007), Tie channels, PhD thesis, Univ. of Calif., Berkeley.
- Rowland, J. C., M. T. Stacey, and W. E. Dietrich (2009), Turbulent characteristics of a shallow wall-bounded plane jet: Experimental implications for river mouth hydrodynamics, *J. Fluid Mech.*, 627, 423–449, doi:10.1017/S0022112009006107.
- Rowland, J. C., W. E. Dietrich, and M. T. Stacey (2010), Morphodynamics of subaqueous levee formation: Insights into river mouth morphologies arising from experiments, *J. Geophys. Res.*, 115, F04007, doi:10.1029/2010JF001684.
- Syvitski, J. P. M., and Y. Saito (2007), Morphodynamics of Deltas under the Influence of Humans, *Global Planet. Change*, 57, 261–282.
- Syvitski, J. P. M., K. Skene, M. Nicholson, and M. Morehead (1998), Plume 1.1: Deposition of sediment from a fluvial plume, *Comput. Geosci.*, 24(2), 159–171.
- Syvitski, J. P. M., et al. (2009), Sinking deltas due to human activities, *Nat. Geosci.*, 2, 681–686.
- van Rijn, L. C. (1986), Mathematical modeling of morphological processes in the case of suspended sediment transport, *J. Hydraul. Eng.*, 112, 433–455.
- Wang, F. C. (1984), The dynamics of a river-bay-delta system, *J. Geophys. Res.*, 89(C5), 8054–8060.
- Wood, R. B., and M. E. A. McIntyre (2010), A general theorem on angular-momentum changes due to potential vorticity mixing and on potential-energy changes due to buoyancy mixing, *J. Atmos. Sci.*, 67, 1261–1274.
- Wright, L. D. (1977), Sediment transport and deposition at river mouths: A synthesis, *Geol. Soc. Am. Bull.*, 88(6), 857–868.